Optical and Electrical Properties of Tin-Doped Cadmium Oxide Films Prepared by Electron Beam Technique

H. M. Ali*, H. A. Mohamed†, M. M. Wakkad, and M. F. Hasaneen

Physics Department, Faculty of Science, Sohag University, Sohag 82524, Egypt

Received March 27, 2008; accepted June 20, 2008; published online April 20, 2009

Tin-doped cadmium oxide films were deposited by electron beam evaporation technique. The structural, optical and electrical properties of the films were characterized. The X-ray diffraction (XRD) study reveals that the films are polycrystalline in nature. As composition and structure change due to the dopant ratio and annealing temperature, the carrier concentration was varied around $10^{20}\,cm^{-3}$, and the mobility increased from less than 10 to $45\,cm^2\,V^{-1}\,s^{-1}$. A transmittance value of ~83% and a resistivity value of $4.4 \times 10^{-4}\,\Omega\,cm$ were achieved for $(CdO)_{0.88}(SnO_2)_{0.12}$ film annealed at 350 °C for 15 min., whereas the maximum value of transmittance ~93% and a resistivity value of $2.4 \times 10^{-3}\,\Omega\,cm$ were obtained at 350 °C for 30 min. The films exhibited direct band-to-band transitions, which corresponded to optical band gaps of 3.1–3.3 eV.

DOI: 10.1143/JJAP.48.041101

1. Introduction

Transparent conducting oxides (TCOs) are used extensively for a variety of applications, including architectural windows, flat-panel displays, thin-film photovoltaics, electrochromic windows, and polymer-based electronics.[1–3] These transparent, metallic oxides include, in part, indium oxide, tin oxide, indium tin oxide, zinc oxide, and cadmium tin oxide.

Cadmium tin oxide (CTO), the ternary TCO material, is a transparent conductor material that combines many beneficial characteristics of both SnO_2 and CdO. It is an n-type semiconductor with either orthorhombic or spinel crystal structure.[4] The ratio of Cd and Sn cations becomes important for obtaining a TCO film.

Tin doped CdO thin films have been synthesized by various techniques, including chemical bath deposition (CBD),[5] activated reactive evaporation,[6] spray pyrolysis,[7,8] rf sputtering,[9,10] metal–oxide chemical-vapor deposition (MOCVD),[11] and pulsed laser deposition (PLD).[12]

Electron beam evaporation is a thin-film deposition technique that has produced high-quality films in a variety of different material systems, and provides economical and efficient usage of evaporant.[13,14]

The aims of work are (1) to carry out experimental studies of the structural, optical, and electrical properties of the transparent-conductive film of tin doped cadmium oxide deposited by electron beam evaporation technique, (2) enhancement of the optical and electrical properties of the TCO materials used in solar cells, thereby to improve the overall performance of the TCO materials, and (3) to predict the selective properties of transparent conductive coatings from the fundamental optical and electrical properties.

2. Experimental Procedure

2.1 Preparation of bulk initial materials

Appropriate proportions of highly pure (99.999%) CdO and SnO_2 powders were ground separately by means of an agate mortar and pestle. Mixtures of CdO and SnO_2 have been used to prepare $(CdO)_{1-x}(SnO_2)_x$ with $x = 0.05$, 0.1, 0.12, 0.15, and 0.2 wt %. To increase complete mixing, the mixtures were ground for at least three hours. Then, they have been made in tablets form using a cold pressing technique. For this purpose, a stainless-steel die with the required internal diameter was used.

Sintering process on the tablets was carried out in the temperature range, $T_M/2 \leq T \leq T_M$, where T_M is the melting point of the material to be sintered.[15] This process was performed for the present mixtures at 800 °C for 3 h.

2.2 Preparation of thin films

In the present work, thin films of the prepared $(CdO)_{1-x}(SnO_2)_x$ ($x = 0.05$, 0.10, 0.12, 0.15, and 0.2 wt %) tablets were deposited from a single source using electron beam evaporation technique onto ultrasonically cleaned microscopic glasses using an Edwards high vacuum coating unit model E306A. The deposition conditions were: (1) a vacuum of 2.66×10^{-3} Pa (2×10^{-5} Torr), (2) an accelerating voltage of 3 kV, (3) electron beam current 8–14 mA. The film thickness (~150 nm) and deposition rate (10 nm/min) were controlled by means of a digital film thickness monitor model TM200 Maxtek.

2.3 Film annealing

The annealing process is considered one of the important factors that affect the physical properties of thin film materials. The annealing temperature from 150 to 500 °C for 15 min and the annealing time from 15 to 180 min at fixed temperature of the deposited films were carried out in a fully controlled furnace in air.

2.4 Film characterization

2.4.1 X-ray diffraction investigation

To reveal the crystal structure of as-deposited films of the studied samples and their change due to annealing temperature and time, the films have been examined using X-ray diffraction (XRD; Philips model PW1710 with Cu as target and Ni as filter, $\lambda = 1.5418$ Å, Holland) by varying the diffraction angle 2θ from 4 to 70° by step width of 0.04.

2.4.2 Atomic force microscopy

The surface morphology of $(CdO)_{1-x}(SnO_2)_x$ thin films was examined by atomic force microscopy (AFM) using a commercial instrument (Nanotec Electronica SL) working in the tapping mode. Etched single-crystalline silicon nitride tips with a nominal end radius of 10 nm and a spring

*E-mail address: hazem95@yahoo.com
†Present address: Physics Department, Teachers College, King Saud University, 11148 Riyadh, KSA.

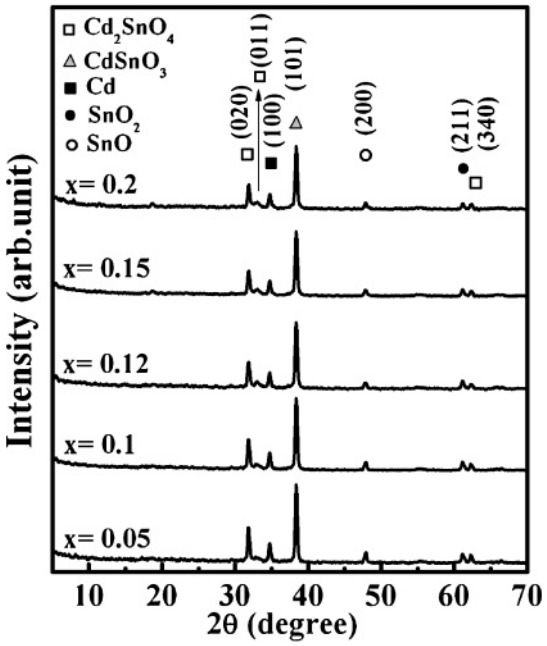

Fig. 1. Typical XRD patterns of as-deposited $(CdO)_{1-x}(SnO_2)_x$ films with x = 0.05, 0.1, 0.12, 0.15, and 0.2.

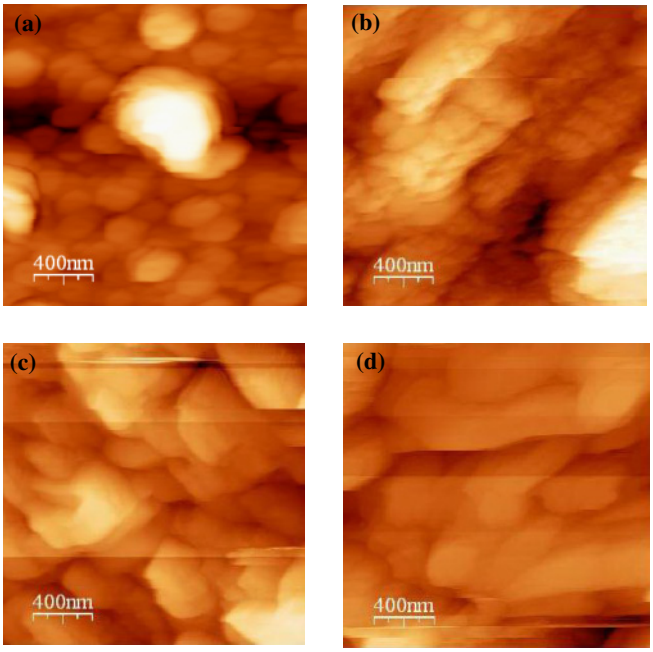

Fig. 2. (Color online) AFM images (surface areas of 4 x 4 μm^2) of $(CdO)_{1-x}(SnO_2)_x$ thin films with x = 0 (a), 0.05 (b), 0.12 (c), and 0.2 (d).

constant of 0.76 N/m were used with scan rates of 0.86 lines per second. Data were taken at 512 points per scan line.

2.5 Optical measurements

Both transmittance and reflectance of $(CdO)_{1-x}(SnO_2)_x$ thin films have been measured by means of a computer-programmable Jasco V-570 double beam spectrophotometer in the wavelength range from 200 to 2500 nm at normal incidence with a scan speed of 1000 nm/min. Spectra were recorded at room temperature. In the case of reflectivity measurement, an additional attachment model ISN-470 was provided.

2.6 Film resistivity measurements

Measurements of film resistance at room temperature were performed by means of a digital Keithley 614 electrometer using two-probe technique. Electrical contacts were made by applying silver paste over the surface of the films with a separation of 2 mm.

3. Results and Discussion

3.1 As-deposited $(CdO)_{1-x}(SnO_2)_x$ films

3.1.1 Film structure

Typical XRD patterns of as-deposited $(CdO)_{1-x}(SnO_2)_x$ films with $x = 0.05$, 0.1, 0.12, 0.15, and 0.2 are shown in Fig. 1. The patterns reveal that all films are polycrystalline with preferred orientation along (020), (011), and (340) planes indicating to the formation of Cd_2SnO_4 and diffraction with (101) plane referring to the presence of another phase of $CdSnO_3$. Both Cd_2SnO_4 and $CdSnO_3$ are two known phases of CTO, whereas their compositional behaviour is more exciting and interesting when they are brought together. Both these compounds possess an orthorhombic crystal structure and are n-type semiconductors.[16] The diffraction peak of Cd element associated with (100) plane is observed in the pattern, indicating a large oxygen deficiency. Small diffraction peaks of SnO(200) and SnO_2(211) have been observed. A small shift of ~0.1° in the position of $CdSnO_3$ diffraction peak was observed, which is most likely due to a slight change in the lattice parameter associated with (1) oxygen vacancies, (2) Sn substitutes, and/or (3) stress.[11,17]

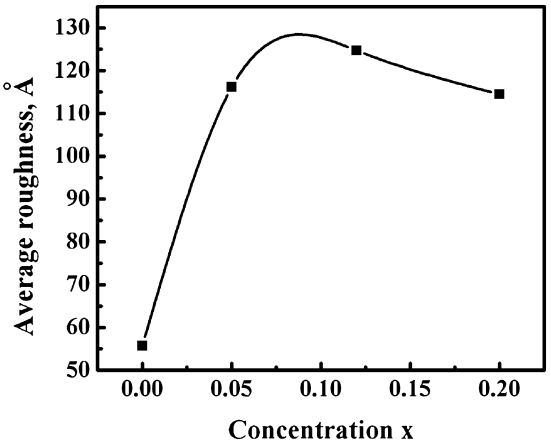

Fig. 3. The average surface roughness of as-deposited $(CdO)_{1-x}(SnO_2)_x$ thin films with x = 0, 0.05, 0.12, and 0.2.

The AFM images of as-deposited 150-nm-thick $(CdO)_{1-x}(SnO_2)_x$ thin films, $x = 0$, 0.05, 0.12, and 0.2 represented in Fig. 2. It is evident that, the particles size increases with increasing SnO_2 content up to $x = 0.12$. For further increase in x ratio the particle size decreases, indicating that the surface roughness of the films is changed with increasing the doping. The average surface roughness of films is shown in Fig. 3. A considerable increase in the surface roughness is observed in the films with increasing Sn content up to $x = 0.12$; for further increase in Sn content the surface roughness slightly decreased due to the decrease in the particle size. The extremely high surface roughness is attributed to the crystalline structure of the films.

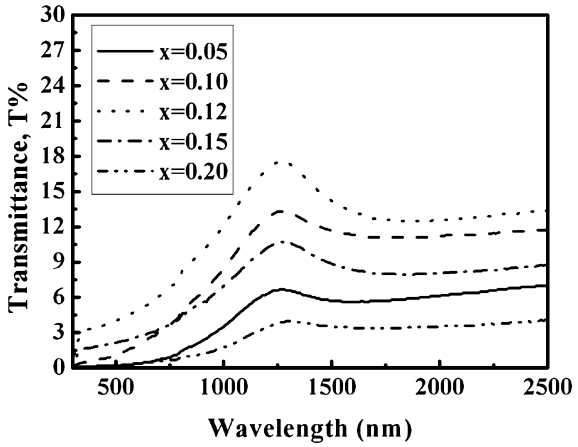

Fig. 4. The transmittance (T%) spectra of 150-nm-thick as-deposited tin-doped cadmium oxide films for different concentration of tin oxide x.

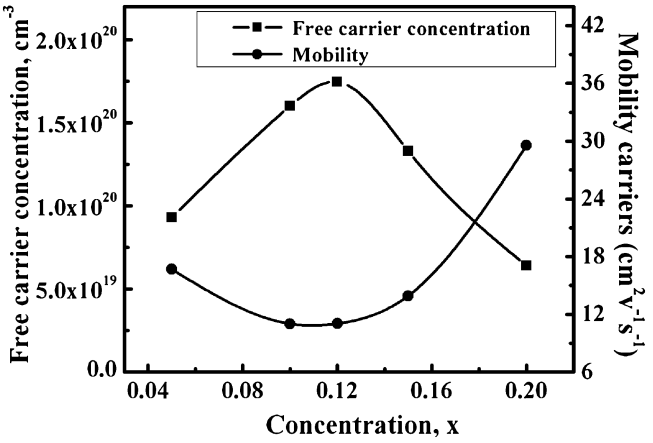

Fig. 5. Plot of the free carrier concentration and carrier mobility estimated from the optical measurements for as-deposited $(CdO)_{1-x}(SnO_2)_x$ thin films with $x = 0.05$, 0.10, 0.12, 0.15, and 0.2.

3.1.2 Optical and electrical properties

Figure 4 depicts the transmittance (T%) spectra of 150-nm-thick as-deposited tin-doped cadmium oxide films for different concentration of tin oxide x in the wavelength range from 200 to 2500 nm. It was observed that, all films show poor optical transmittance either in visible or near infrared regions, which can be attributed to the oxygen deficiency[3,18] or due to the high value of the surface roughness of the films due to increased optical scattering of incident light on the film surface.[19] It is evident also that the transmittance increases to reach its maximum value at $x = 0.12$ and after that decreased gradually with increasing x ratio.

The classical Drude free-electron theory can be used to explain the optical phenomenon near the infrared region. Despite the fact that the classical Drude free-electron theory has been superseded by quantum theory many years ago, it works quite well for TCOs.[20] The concentration of free electrons is calculated using Drude's theory of dielectrics as follows:

The real dielectric constant (ε') can be written as:[13,21]

$$\varepsilon' = n^2 - k^2 = \varepsilon_i - \frac{e^2}{4\pi^2 c^2 \varepsilon_0}\left(\frac{N}{m^*}\right)\lambda^2 \quad (1)$$

and

$$\frac{e^2}{\pi c^2}\left(\frac{N}{m^*}\right)\lambda^2 = -4\pi\chi_c, \quad (2)$$

where ε_i is the infinitely high frequency dielectric constant or the residual dielectric constant due to the ion core, N/m^* is the ratio of carrier concentration to the effective mass, χ_c is the electric free carrier susceptibility and e is the elementary charge (1.6×10^{-19} C).

Values of the carrier mobility (μ) were calculated using the following equation:[22]

$$\mu = \frac{1}{Ne\rho}. \quad (3)$$

The behavior of carrier concentration and carrier mobility is shown in Fig. 5. It is evident that the carrier concentration increases up to $x = 0.12$ and after that decreases with further increase in x ratio. The decrease of free carrier concentration is related to the decrease of oxygen vacancies as shown in the XRD pattern, since the intensity of (100) free cadmium decreases with further increasing of tin dopants. On the other hand, the decrease in the carrier mobility up to $x = 0.12$ is due to the increase of the surface roughness of the films, Meanwhile the increase in the carrier mobility for heavily doped cadmium oxide can be attributed to the decrease in the free carrier concentration and the surface roughness of the films.

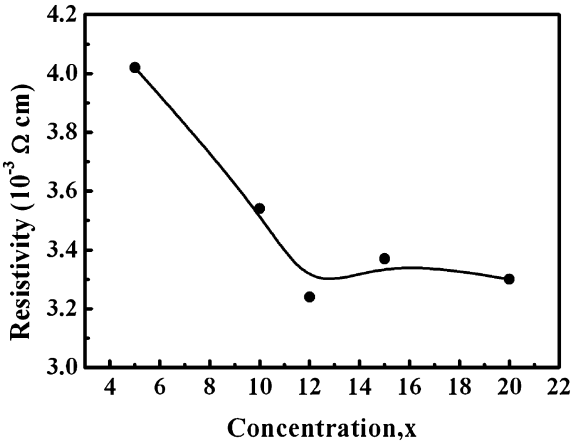

Fig. 6. Variation of the electrical resistivity with x concentration of as-deposited $(CdO)_{1-x}(SnO_2)_x$ thin films with $x = 0.05$, 0.10, 0.12, 0.15, and 0.2.

Figure 6 shows the electrical resistivity ρ of the as-deposited films. It is clear that the resistivity decreased with increasing SnO_2 content. The decrease in the film resistivity is very likely due to the behaviour of the free carrier concentration and the carrier mobility that were discussed above.

3.2 Effect of annealing temperature on $(CdO)_{1-x}(SnO_2)_x$ films

3.2.1 Film structure

Upon determination of an optimum Cd to Sn ratio, the effect of the annealing temperature in air on the structural, optical and electrical properties were investigated for $(CdO)_{1-x}(SnO_2)_x$ film with $x = 0.12$.

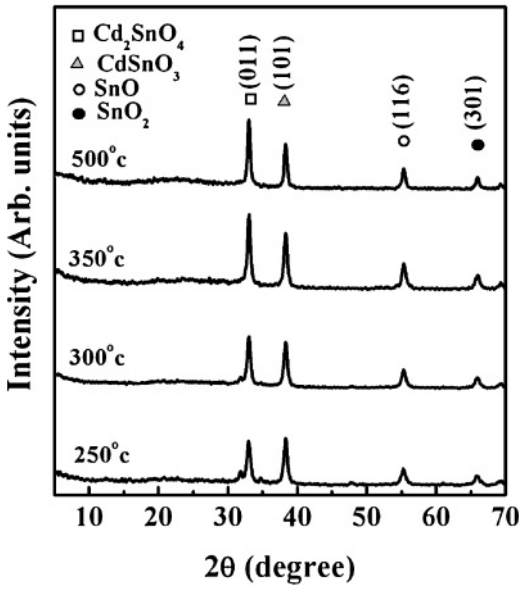

Fig. 7. XRD patterns of $(CdO)_{0.88}(SnO_2)_{0.12}$ films annealed at different temperatures.

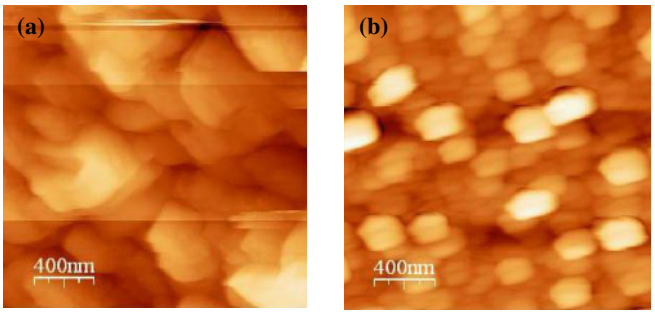

Fig. 8. (Color online) AFM images (surface areas of 4 × 4 μm^2) of $(CdO)_{0.88}(SnO_2)_{0.12}$ film: (a) as-deposited and (b) annealed at 350 °C.

The crystal structure changes in the CTO films, due to an increase in the post-deposition annealing, were determined from XRD analysis depicted in Fig. 7. It is observable that, all films of CTO exhibit a polycrystalline nature, displaying prominent diffraction peaks at $2\theta = 33.04°$ and 38.4°, corresponding to the $Cd_2SnO_4(011)$ and $CdSnO_3(101)$ crystal planes. On increasing the temperature of annealing the intensity of $CdSnO_3(101)$ decreases while that of the $Cd_2SnO_4(011)$ diffraction peak increases. It is obvious that all atoms of Sn oxidized and Sn-diffraction peak disappeared. Beside, diffraction peaks of (116) and (301) corresponding to the presence of SnO and SnO_2 respectively can be observed. The presence of SnO and SnO_2 means that tin exists in two oxidation states, Sn^{+2} and Sn^{+4} respectively. The XRD pattern shows a small concentration of SnO_2 associated with (301) plane.

AFM images as given in Fig. 8 show the influence of annealing temperature on the structural properties of $(CdO)_{1-x}(SnO_2)_x$ thin films with $x = 0.12$. It was found that, the surface roughness of annealed film at 350 °C is equal to 22.4 Å whereas the surface roughness of as-deposited film is equal 124.7 Å.

3.2.2 Optical and electrical properties

Figure 9 illustrates the transmittance spectra of

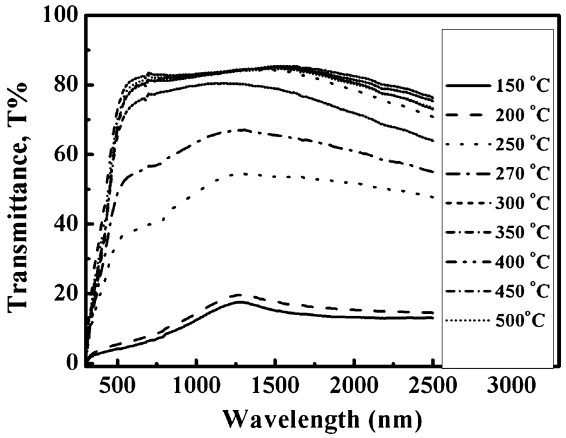

Fig. 9. Spectral variation of the transmittance *T*% with wavelength of $(CdO)_{0.88}(SnO_2)_{0.12}$ film for different annealing temperature for 15 min.

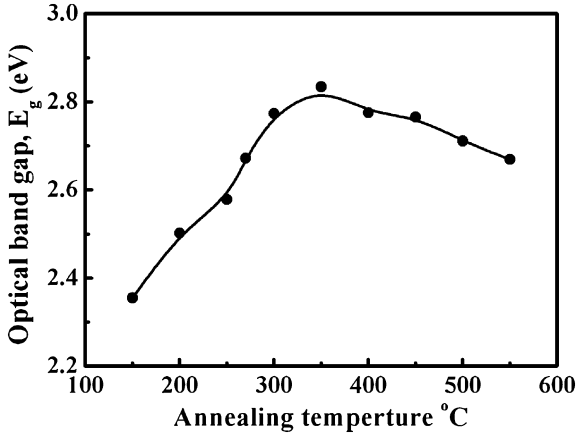

Fig. 10. Annealing temperature dependence of the optical energy gap of $(CdO)_{0.88}(SnO_2)_{0.12}$ film as a function of annealing temperature.

$(CdO)_{1-x}(SnO_2)_x$ thin films with $x = 0.12$ annealed at different temperatures. It is evident that the transmittance increases with increasing the temperature of annealing and the maximum value of transmittance is achieved for annealed film at 350 °C, whereas the transmittance in the visible region exceeds 83%. The increase in the film transmittance with annealing temperature can be attributed to the incorporation of oxygen and to the formation of the Cd_2SnO_4 phase, which is increased with increasing the temperature of annealing as shown in the XRD pattern. From the previous result, we can conclude that the Cd_2SnO_4 phase is responsible for enhancing the transmittance and $CdSnO_3$ phase is responsible for enhancing the conductivity of the films. Such a shift in the absorption edge towards the blue region is observed. It is assumed that this shift of the absorption edge towards higher energy resulted from the increase in carrier concentration in accordance with the Moss–Burstein effect,[23] indicating a continuous increase in the energy gap up to 350 °C, as shown in Fig. 10. The decrease in the optical energy gap above 350 °C arises from the decrease in the free carrier concentration. The variation of free carrier concentration and electrical resistivity of $(CdO)_{0.88}(SnO_2)_{0.12}$ thin films with annealing

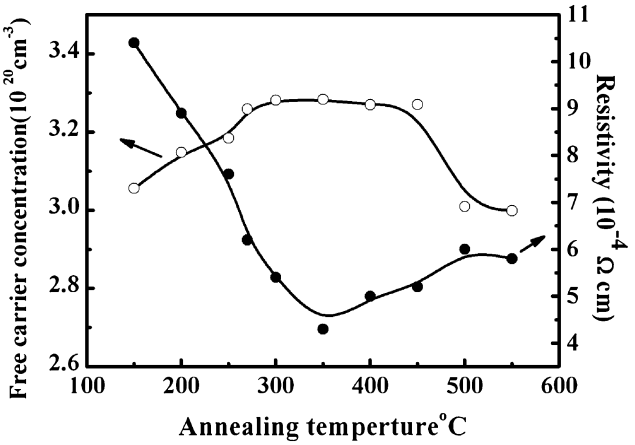

Fig. 11. Variations of the free carrier concentration and the electrical resistivity of $(CdO)_{0.88}(SnO_2)_{0.12}$ film with annealing temperature for 15 min.

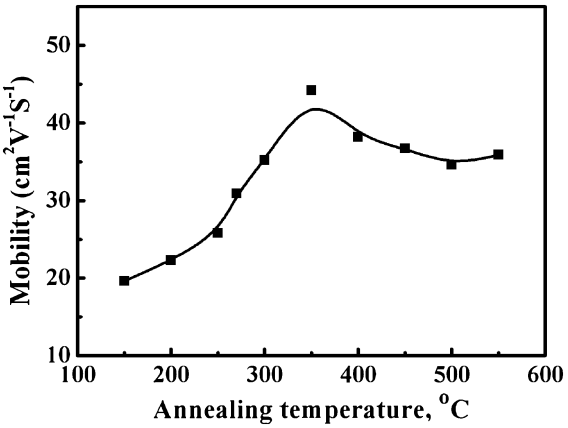

Fig. 12. The carrier mobility of $(CdO)_{0.88}(SnO_2)_{0.12}$ film as a function of annealing temperature for 15 min.

temperature is depicted in Fig. 11. It is seen that the resistivity of the films decreases with increasing the temperature of annealing up to 350 °C and it begins to increase at higher temperatures. The optimum temperature of annealing at which the lowest resistivity occurred was at 350 °C. The decrease of the film resistivity up to 350 °C can be attributed to the increase of the free carrier concentration, whereas the increase of the film resistivity for annealing temperature above 350 °C arises from the decrease of the free carrier concentration. When the films are annealed under ambient air at temperature higher than 350 °C, oxygen is chemisorbed on the film surface and in pores, acting as an acceptor by accepting an electron from occupied conduction band states.[24] Furthermore, the adsorbed oxygen removes tin interstitials and/or oxygen vacancies, thus reduces the density of donors like defects and carrier concentration,[25,26] leading to an increase in the electrical resistivity.

Figure 12 shows the annealing temperature dependence of carrier mobility. The figure indicates the increase of the carrier mobility with increasing temperature of annealing up to 350 °C and after that it slightly decreased at higher temperatures.

The unexpected feature of all films is an increase of the carrier mobility with increasing the free carrier concentration, which contradicts the semiconductor theory for homogeneous samples with high carrier concentrations. It therefore appears likely that the electrical properties of these films do not reflect the properties of Cd_2SnO_4 but are largely determined by their multiphase composition.[25]

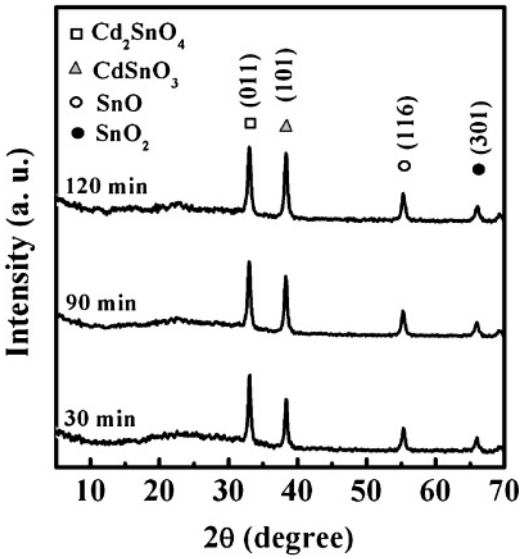

Fig. 13. XRD patterns of $(CdO)_{0.88}(SnO_2)_{0.12}$ films annealed at 350 °C for different times.

From the previous data it is clear that the optimum annealing temperature at which the lowest resistivity (4.3×10^{-4} Ω cm) and highest transmission (~80%) is occurred, is $T_{ann} = 350$ °C.

3.3 Effect of annealing time

3.3.1 Film structure

Figure 13 shows the XRD patterns of $(CdO)_{0.88}(SnO_2)_{0.12}$ thin film annealed at 350 °C for different times within 2θ range of angles between 4 and 70° by XRD. The diffraction patterns indicate that the films are polycrystalline in nature. Prominent diffraction peaks (011) and (101) are observed in the patterns indicating the presence of Cd_2SnO_4 and $CdSnO_3$ respectively. A slight shift (~0.12°) of diffraction peak of $CdSnO_3$ is observed, which most likely due to a slight change in the lattice constant. Another two diffraction peaks of (116) and (301) corresponding to the presence of SnO and SnO_2 respectively can be observed.

The AFM images of $(CdO)_{0.88}(SnO_2)_{0.12}$ thin film annealed at 350 °C for different times are shown in Fig. 14. A surface roughness study demonstrated that the surface roughness and the particle size increase with increasing the time of annealing. It was probably due to the better crystallinity formed after increasing the time of annealing.

3.3.2 Optical and electrical properties

Figure 15(a) exhibits the ultraviolet–visible–near infrared (UV–vis–NIR) transmission spectra of $(CdO)_{0.88}(SnO_2)_{0.12}$ films annealed at 350 °C for different time periods. For all annealed films, it is evident that the transmission improved substantially with increasing the time of annealing and goes up to 92% in the visible region. A slight loss in transmission

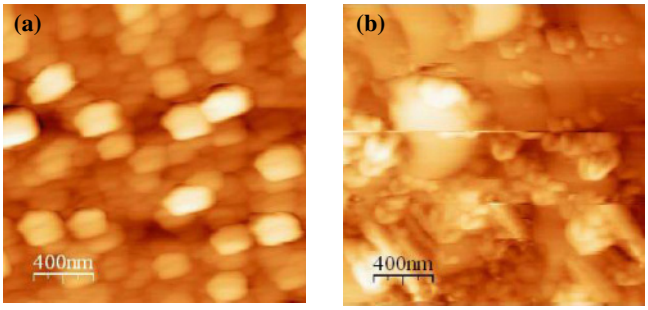

Fig. 14. (Color online) AFM images (surface areas of 4 × 4 μm^2) of $(CdO)_{0.88}(SnO_2)_{0.12}$ films annealed at 350 °C for (a) 15 and (b) 45 min.

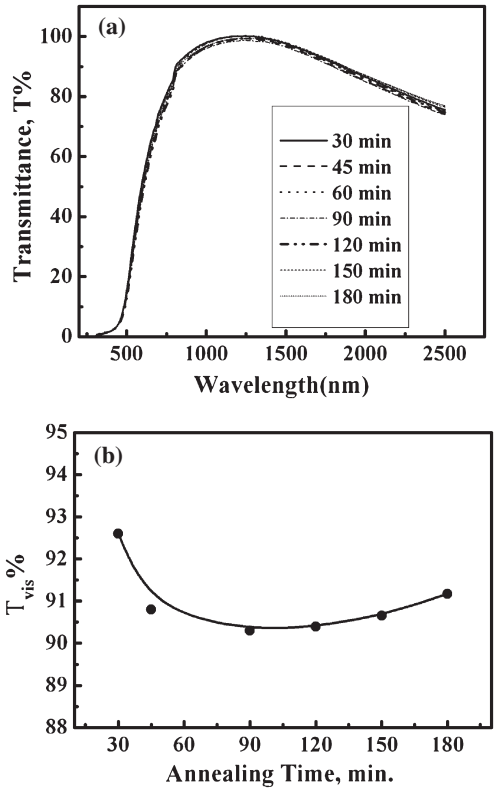

Fig. 15. Spectral variation of the transmittance *T*% with wavelength of $(CdO)_{0.88}(SnO_2)_{0.12}$ film annealed at 350 °C for different times (a) and the average transmittance in the visible region (b).

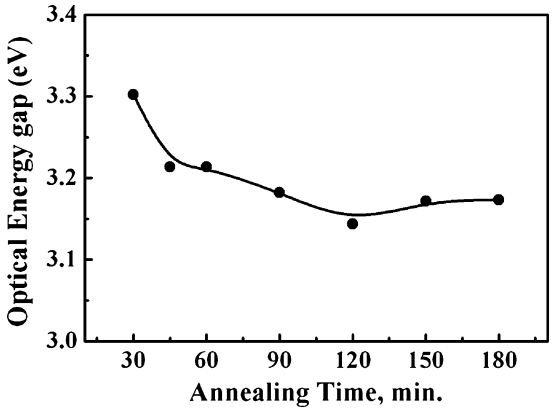

Fig. 16. Annealing time dependence of optical energy gap of $(CdO)_{0.88}(SnO_2)_{0.12}$ film.

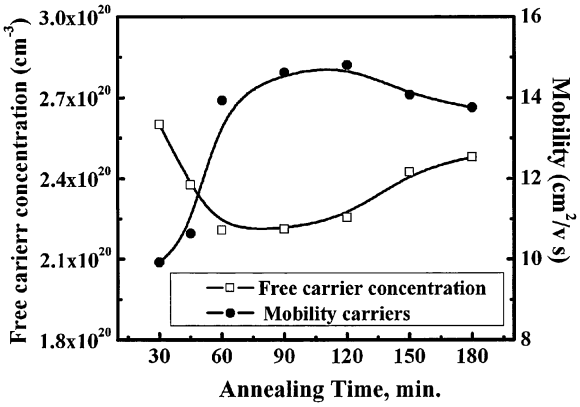

Fig. 17. The free carrier concentration and carrier mobility of $(CdO)_{0.88}(SnO_2)_{0.12}$ film annealed at 350 °C for different times.

in the visible region resulting from the increase in the time of annealing can be observed in Fig. 15(b). This decrease may be attributed to the charge transfer between the two oxidation Sn^{4+} and Sn^{2+} states of tin. A little shift in the transmittance threshold to higher wavelengths as increasing the time of annealing is also observed, and this leads to decrease the energy band gap as shown in Fig. 16.

The calculated values of the free carrier concentrations and the carrier mobility belonging to these films are shown in Fig. 17. A decrease in carrier concentration with increasing the time of annealing up to 60 min is afforded by the annealing out of point defects and interstitial impurities.[10,16] The increase of carrier concentration with increasing the time of annealing above 60 min can be interpreted by part of the Cd^{2+} atoms in the lattice of Cd_2SnO_4 being replaced by Sn^{4+}: this part of the cadmium diffuses into $CdSnO_3$ lattice to form interstitial donors. This assumption is supported by the increase in lattice constant resulting a shift in the diffraction peak of $CdSnO_3$, which is produced in the XRD pattern in Fig. 13, because the ionic radius of Cd^{+2} is greater than that of Sn^{+4}. The increase in carrier concentration can be attributed also to the increase of $CdSnO_3$ and SnO on account of Cd_2SnO_4 and SnO_2 phases respectively as seen in Fig. 13. On the other hand, Fig. 17 shows that the carrier mobility increases with time of annealing from less than 10–14.5 cm^2 V^{-1} s^{-1}.

Variation of the electrical resistivity with annealing time can be observed in Fig. 18, which shows that the resistivity decreases with increasing the time of annealing. This can be partly attributed to the increase of $CdSnO_3$ and SnO phases as seen in Fig. 13. Also, the free carrier concentration contributes to the decrease in the film resistivity.

4. Conclusions

Tin doped cadmium oxide $(CdO)_{1-x}(SnO_2)_x$ thin films have been prepared using electron beam evaporation technique. It was established that, all as-deposited films show poor optical transmittance either in visible or near infrared regions, whereas the electrical resistivity was in the range $(3.22–4.3) \times 10^{-3}$ Ω cm. It was found that the optimum ratio of tin oxide is 0.12. The effect of annealing temperature and time has been studied to optimize the optical and

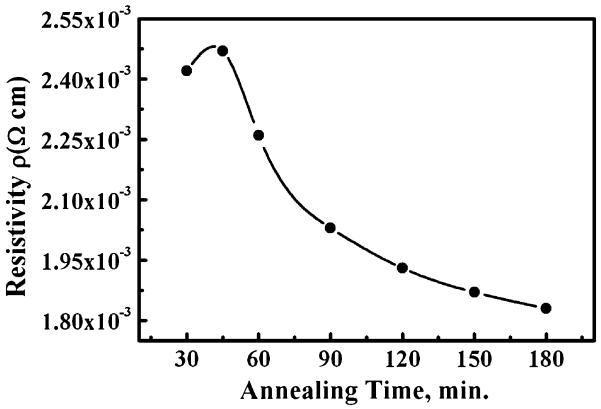

Fig. 18. Variation of the electrical resistivity of $(CdO)_{0.88}(SnO_2)_{0.12}$ film with annealing time.

electrical properties of $(CdO)_{0.88}(SnO_2)_{0.12}$ films. A transmittance value of ~83% and a resistivity value of $4.4 \times 10^{-4}\,\Omega\,cm$ have been achieved for $(CdO)_{0.88}(SnO_2)_{0.12}$ film annealed at 350 °C for 15 min., whereas the maximum value of transmittance ~93% and a resistivity value of $2.4 \times 10^{-3}\,\Omega\,cm$ have been obtained at 350 °C for 30 min. No significant change in the transmittance has been observed with further increase in the time of annealing. As composition and structure change due to the dopant ratio and annealing temperature, the carrier concentration varies around $10^{20}\,cm^{-3}$, and the mobility increases from less than 10 to $45\,cm^2\,V^{-1}\,s^{-1}$. The carrier concentrations and carrier motilities were estimated optically using the Drude model. The films exhibited direct band-to-band transitions, which corresponded to optical band gaps of 3.1–3.3 eV.

Acknowledgment

The authors would like to thank Dr. S. H. Mohamed for performing the atomic force microscope analysis in Berkeley National Laboratory, U.S.A.

1) B. Saha, R. Thapa, and K. K. Chattopadhyay: Solid State Commun. **145** (2008) 33.
2) M. Kul, A. S. Aybek, E. Turan, M. Zor, and S. Irmak: Sol. Energy Mater. Sol. Cells **91** (2007) 1927.
3) H. M. Ali: Phys. Status Solidi A **202** (2005) 2742.
4) X. Li, T. A. Gessert, and T. Coutts: Appl. Surf. Sci. **223** (2004) 138.
5) L. R. de León-Gutiérrez, J. J. Cayente-Romero, J. M. Peza-Tapia, E. Barrera-Calva, J. C. Martínez-Flores, and M. Ortega-López: Mater. Lett. **60** (2006) 3866.
6) G. Phatak and R. Lal: Thin Solid Films **245** (1994) 17.
7) M. T. Mohammad and W. A. S. Abdul Ghafor: Solid State Commun. **88** (1993) 227.
8) A. Abrutis, G. Valincius, G. Baltrunas, L. Parafionovic, A. Valiuniene, and Z. Saltyte: Thin Solid Films **515** (2007) 6817.
9) R. Mamazza, Jr., D. Morel, and C. Ferekides: Thin Solid Films **484** (2005) 26.
10) W. Wohlmuth and I. Adesida: Thin Solid Films **479** (2005) 223.
11) Z. Zhao, D. L. Morel, and C. S. Ferekides: Thin Solid Films **413** (2002) 203.
12) E. Martin, M. Yan, M. Lane, J. Ireland, C. Kannewurf, and R. H. Chang: Thin Solid Films **461** (2004) 309.
13) E. K. Shokr, M. M. Wakkad, H. A. Abd El-Ghanny, and H. M. Ali: J. Phys. Chem. Solids **61** (2000) 75.
14) H. M. Ali, M. M. Abd El-Raheem, N. M. Megahed, and H. A. Mohamed: J. Phys. Chem. Solids **67** (2006) 1823.
15) E. Kh. Shokr, M. M. Wakkad, H. A. Abd El-Ghanny, and H. M. Ali: Eur. Phys. J. Appl. Phys. **8** (1999) 215.
16) T. O. Mason, G. B. Gonzalez, D. R. Kammler, N. Mansourian-Hadavi, and B. J. Ingram: Thin Solid Films **411** (2002) 106.
17) H. M. Ali, H. A. Mohamed, M. M. Wakkad, and M. F. Hasaneen: Thin Solid Films **515** (2007) 3024.
18) R. Thielsch, A. Gatto, J. Heber, and N. Kaiser: Thin Solid Films **410** (2002) 86.
19) D. C. Paine, T. Whitson, and C. O. Yang: J. Appl. Phys. **85** (1999) 8445.
20) T. J. Coutts, D. L. Young, and X. Li: MRS Bull. **25** (2000) No. 8, 58.
21) W. G. Spitzer and H. Y. Fan: Phys. Rev. **106** (1957) 882.
22) H. Haitjema and J. J. Ph. Elich: Thin Solid Films **205** (1991) 93.
23) E. Burstein: Phys. Rev. **93** (1954) 632.
24) H. A. Mohamed, H. M. Ali, S. H. Mohamed, and M. M. Abd El-Raheem: Eur. Phys. J. Appl. Phys. **34** (2006) 7.
25) Y.-S. Choi, C.-G. Lee, and S. M. Cho: Thin Solid Films **289** (1996) 153.
26) I. H. Kim, J. H. Ko, D. Kim, K. S. Lee, T. S. Lee, J.-H. Jeong, B. Cheong, Y.-J. Baik, and W. M. Kim: Thin Solid Films **515** (2006) 2475.